NOISE SOURCE LOCALIZATION IN CLOSED TEST SECTIONS WITH MICROPHONE ARRAYS

L. Koop* P.Sijtsma#, S. Oerlemans#
*German Aerospace Center DLR, 37073 Goettingen, Germany
National Aerospace Laboratory NLR, 8300 AD Emmeloord, The Netherlands

ABSTACT

In order to meet the objectives of ACARE Vision 2020 which aims amongst others at a reduction in perceived noise to one half of current average levels aero-acoustic testing methods must improve considerably. With the advent of the phased array microphone technologies and advanced data processing several research groups have developed the capability to perform acoustic tests within closed-test-section wind tunnels. This paper gives an overview of the current state of the art in microphone array techniques at various European research establishments. Based on these results future developments driven by the industrial requirements will be outlined. The main objective in this context is the extrapolation of results obtained from wind tunnel measurement to real flight conditions.

1. INTRODUCTION

In the last decade, phased array measurements have been increasingly used for the locating of aero acoustic sources on aircraft models. By means of a large number of microphones which are usually placed in a two dimensional plane the source distribution on the model can be calculated and illustrated in so called source maps. The main advantage of this technique with respect to single microphone measurements is that contributions coming from different source directions can be separated from each other and from background noise. Therefore, measurements with a microphone array can even be performed in wind tunnels with a high background noise level.

Aerodynamic measurements are often performed in wind tunnels with closed test sections and acoustically hard side-walls. In these wind tunnels the aerodynamic boundary conditions are well defined and ideal for a comparison with numerical simulations. To increase efficiency and productivity it is desirable to have aero acoustic and aerodynamic measurements in parallel.

Microphone array measurements give the opportunity to combine aerodynamic and aero acoustic tests in closed test section as the background noise is reduced by the array analysis. This has been shown by a number of experiments [1], [2], [3], [4]. In this way, the sound radiation of an aircraft model can be measured already during the design process. Besides different noise reduction measures can be investigated in a very early stage of the development. Other advantages of microphone array measurements in the closed test sections are: Higher frequency range (up to 55 kHz) than in the open test section case and higher spatial resolution due to the fact that the distance between the model and the array is usually very small.

Nevertheless, there is still potential to improve the accuracy of microphone array measurements in closed test sections. Several European research institutes have therefore worked on this topic in the past decade Ehrenfried [5], Sijtsma [6], Blacodon [7], Koop [12]. The current state-of-the-art in microphone array techniques will be described in the next sections. In section 2 the basic theory for the delay-and-sum beamformer (DSB) in time and frequency domain is derived and the array pattern as the determinant of the array performance is illustrated. The improved array analysis tools are described in section 3. The main activities and achievements so far have been:

- Decrease the influence of the boundary layer pressure fluctuations on the array analysis. Theses pressure fluctuations are caused by the fact that the microphones are installed usually in the side walls of the test section and therefore beneath a turbulent boundary layer (section 3.1).
- Reduction of background noise which consists mainly of upstream propagating waves in the closed test section (section 3.2).
- Increase the spatial resolution of the source maps (section 3.3).
- Ability to extract absolute sound power levels from the source plots (section 3.3).

The comparability between different software codes is another issue which has to be examined. Therefore, a benchmark test has been initiated within the EC funded Network of Excellence *European Windtunnel Association* (EWA, http://www.eu-ewa.aero). The objective of this test is to compare the existing analysis software of different European research institutes (ONERA, NLR, DLR, QinetiQ) on the basis of the same measurement data. From these results a recommendation can be deduced for future microphone array measurements in a closed test section and their analysis. The setup of this measurement will be shown in section 4. In addition, this section summarizes the basic principles in closed test-section measurements, data acquisition and the control of the measurement and the data analysis.

The mid-term objective of these combined efforts is to improve the measurement technique so that far-field data can be extracted from microphone array measurements in a closed test section. In the future the array results should give comparable results to flight measurements with real aircrafts (see also [13]). The activities and developments which are required for this objective are summarised in the concluding section 5.

2. BASIC FORMULATIONS

The standard algorithm to localize noise sources with a microphone array is the delay-and-sum beamformer (DSB). In the next two sections the DSB will be formulated for time-domain and the frequency domain array analysis. In section 2.3 the array pattern as the determinant of the array performance is illustrated.

2.1. DSB in time domain

It is assumed that a point source with uniform directivity is located at the position $\vec{y}_o$. The radiated sound field is recorded with a set of microphones which are located at the positions $\vec{x}_m = (x_m, y_m, z_m)^T$ for $m=1,2,\ldots,M$:

$$p(\vec{x}_m,t) = \frac{1}{4\pi}\frac{q\left(t-\frac{\vec{x}_m-\vec{y}_o}{c}\right)}{|\vec{x}_m-\vec{y}_o|}. \quad (1)$$

The retarded time $\tau_m = t - |\vec{x}_m - \vec{y}_o|/c$ specifies the time at which the signal recoded at time t at the microphone m is radiated from the source position $\vec{y}_o$. The time differences $\Delta T_{m,o} = |\vec{x}_m - \vec{y}_o|/c$ vary between the microphones and are compensated in the delay-and-sum beamformer. Therefore, we assume a potential source or focus position at $\vec{y}_f$. The time shift for this focus position can be calculated by $\Delta T_{m,f} = |\vec{x}_m - \vec{y}_f|/c$. The delayed and summed array output is then given by:

$$z(\vec{y}_f,t) = \frac{1}{M}\sum_{m=1}^{M}\frac{|\vec{x}_m-\vec{y}_f|}{|\vec{x}_m-\vec{y}_o|}q\left(t-\Delta\Theta_{o,f}\right) \quad (2)$$

where $\Delta\Theta_{o,f} = \Delta T_{m,o} + \Delta T_{m.f}$ is the travel-time difference between real source and focus position. Obviously, if the focus position $\vec{y}_f$ coincides with the real source position $\vec{y}_o$ we obtain $z(t) = q(t)$ and for other focus position we will usually get: $|z(t)| < |q(t)|$.

2.2. DSB in frequency domain

If the source does not move with respect to the microphones it is often convenient to perform the delay-and-sum beamformer in the frequency domain. For that purpose the time sequence $p_m(n)$ measured at the microphone with position $\vec{x}_m$ is transformed in the frequency domain:

$$P_m(\omega) = \sum_{n=0}^{N-1} p_m(n)e^{-j\pi nk/N}. \quad (3)$$

The array output in Eq. (2) can be rewritten in the frequency domain as follows:

$$Z(\vec{y}_f,\omega_k) = \frac{1}{M}\sum_{m=1}^{M}\frac{|\vec{x}_m-\vec{y}_f|}{|\vec{x}_m-\vec{y}_o|}Q(\omega_k)e^{-j\omega k\Delta\Theta} \quad (4)$$

where M is the number of microphones. In this case it is also true that if there is a monopole source at the position $\vec{y}_f$ Eq. (4) has a maximum with:

$$Z(\vec{y}_f = \vec{y}_o,\omega_k) = Q(\omega_k). \quad (5)$$

For some considerations it is more convenient to reformulate Eq. (4) in a vector-matrix notation as:

$$Z(\vec{y}_f,\omega_k) = \vec{e}^{\,H}\boldsymbol{W}\,\vec{p} \quad (6)$$

where $()^H$ denotes the conjugate transposed vector or matrix.

In practical applications the signal $\vec{p}$ and therefore the results in Eq. (6) are very noisy due to external disturbances. To reduce this noise the auto power spectrum of the array output is averaged over N samples which can be written according to

$$\hat{S}_{zz}(\omega_k) = \sum_{i=1}^{N} Z_i^*(\omega_k)Z_i^*(\omega_k). \quad (7)$$

This can be summarized with Eq. (6):

$$\hat{S}_{zz}(\omega_k) = \vec{e}^{\,H}\,\boldsymbol{W}\boldsymbol{R}\boldsymbol{W}^{\boldsymbol{H}}\vec{e}^{\,H} \quad (8)$$

where $\boldsymbol{R}$ is the cross spectral density matrix of the measured signal.

2.3. Array pattern and performance

The response of an array to a point source is described by its *array pattern* or *point spread function*. Due to the fact that the sound field is recorded by a finite pressure sensitive field the array pattern shows a main lobe with a finite width and several side lobes. The shape of this array pattern determines the performance of the microphone array. The resolution of a microphone array for example depends on the width of the main-lobe. The height of the side lobes determines the ability of the array to detect a weak sound source in the vicinity of a strong source.

There have been several publications on the optimization of microphone arrangements to achieve a maximum side lobe suppression and a desired resolution in a large frequency range [14], [16], [17]. FIG 1 shows the example of the optimised microphone arrangement of the DLR in-flow array. The microphones

are positioned in a multi-arm spiral array in which the single arms are given by the following equation:

(9) $$r(\theta) = r_o e^{\cot(\nu)\theta}$$

where θ is the polar angle, r is the distance from the origin, r_o is the value of r at $\theta = 0$ and ν is the spiral angle. FIG 2 a) shows the array pattern along the x-axis of this microphone arrangement. The point source with f = 8000 Hz is located in 1 m distance to the array at $\vec{y}_o = (0,0,1)^T$. The main lobe of the array pattern is located at x = 0. The resolution of the array at this frequency is approximately dx = 39 mm. In the outer region several side lobes are visible. Since it is difficult to distinguish between the side lobes of a main source and the main lobes of other sources it is desirable to keep these side lobes as low as possible. The advantage of the logarithmic spiral arrangement can be seen in FIG 2 b) which shows the point spread function for f = 40000 Hz. This result does not show any disturbing side-lobes above −14 dB. The logarithmic spiral arrangement provides an effective side-lobe control over a wide frequency range.

In section 3.3 some examples a given to reduce these side lobe effects and the limited resolution by post-processing techniques.

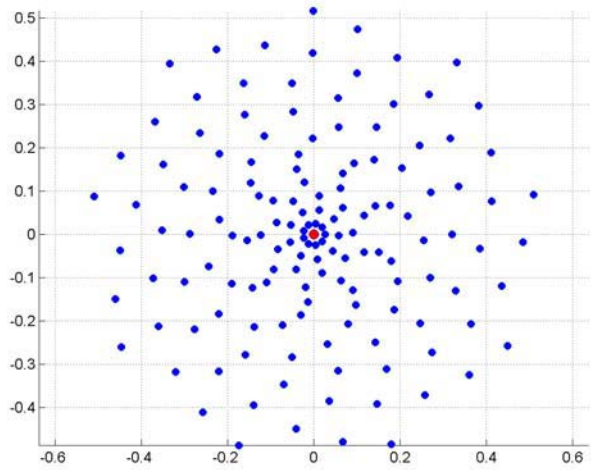

FIG 1. Arrangement of 144 microphones in a two-dimensional plane. The centre of the array is located in the origin.

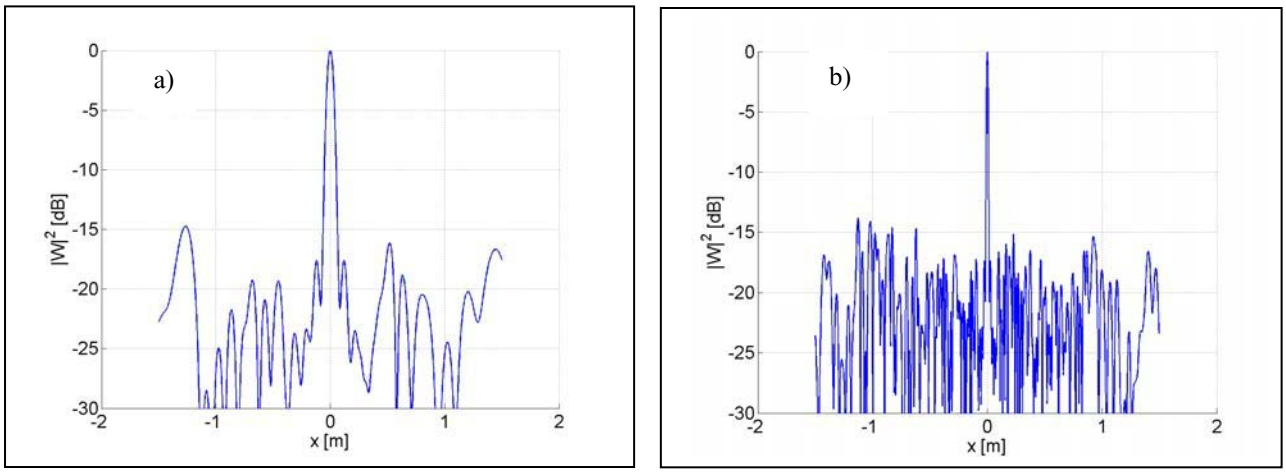

FIG 2. Array Pattern for the microphone arrangement in FIG 1 with a source distance of z_o = 1.0 m. Depicted is the intersection along the x-axis for y = 0.0 m. The source frequency is f = 8000 Hz (left) and f = 40000 Hz (right).

3. IMPROVED ARRAY ANALYSIS

3.1. Diagonal removal

When a microphone is placed in the flow, it will detect not only acoustic pressure fluctuations, but also pressure disturbances of hydrodynamic nature due to the turbulent boundary layer around the microphone. This typically occurs in closed wind tunnel test sections, where the microphones are mounted flush in a wall. Because wind noise is incoherent from one microphone to the other, it will appear only in the auto-power spectra of the microphones, that means on the main diagonal of cross-spectral matrix $\boldsymbol{R}$. As the phase does not enter the terms on the main diagonal they are not essential for the phased array results in Eq. (8). Therefore much cleaner results are obtained when the auto-power spectra are not used in the beamforming process. The calculation of the array output in Eq. (8) can be rewritten in the following form:

(10) $$\hat{S}_{zz}(\omega_k) = \sum_{m=1}^{M} |e_m|^2 R_{mm} + \sum_{m' \neq m} e_m^* R_{mm'} e_{m'}$$

This gives the beamforming expression as two sums, the first involving the diagonal element of the cross-spectral matrix, and the second depending on the off-diagonal elements of the cross-spectral matrix. Using the beamforming algorithm in the closed test-section measurement the first term in Eq.(10) is often neglected. This procedure is called diagonal removal (DR).

Examples of noise source maps obtained without and with diagonal removal are shown in FIG 3. It shows results from a Fokker-100 model in the DNW-LST, which is a closed test section wind tunnel with a contraction ratio of 9 and a maximum velocity of 80 m/s. The dimensions of the test section are: width 3.0 m and height 2.25 m. The improvement in the array performance when DR is applied is clearly visible.

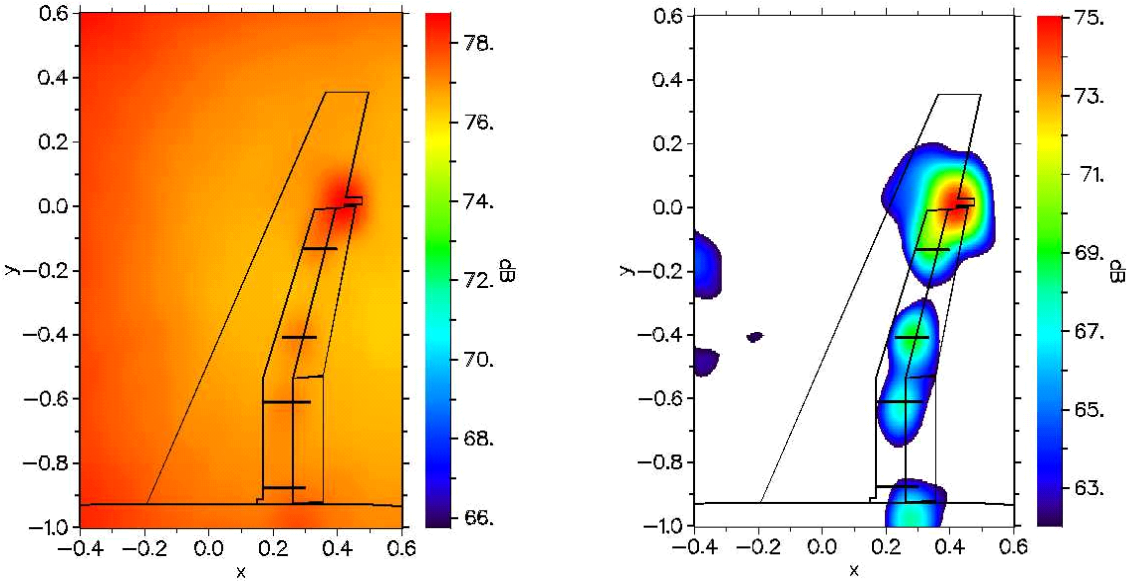

FIG 3. Noise source maps on a Fokker-100 model in DNW-LST (closed), obtained without DR (left) and with DR (right)

3.2. Background noise – BiClean algorithm

In the previous section we have seen that the wall pressure fluctuations generated by the turbulent boundary layer have a small spatial correlation length and therefore only have an effect on the auto power spectra of the microphone signal. The signal-to-noise ratio can be significantly increased by the DR method. Another problem in closed test section measurements is the increased background noise level. Acoustic waves are generated at many locations in the wind tunnel and not only at the model in the test section. Because of the hard side walls the sound waves can propagate almost undamped through the tunnel. This kind of noise generates microphone signals which are correlated all over the array. Thus, the effect of the background noise is not eliminated by the DR approach shown in section 3.1.

The artefacts by the background noise in the array analysis can be reduced effectively by the BiClean algorithm [5]. The idea is, to split up the cross spectral matrix $\boldsymbol{R}$ into a first part $\boldsymbol{R_1}$ which represents the real sources in the observation plane (on the model), and a second part $\boldsymbol{R_2}$ which describes the background noise (mainly upstream-propagating plane waves).

In an iterative procedure matrix $\boldsymbol{R}$ is split into the two sub matrices. In each loop both, a source map according to Eq. (10) and a map in the wave-number space are calculated. Then the absolute maximum over both maps is searched. This maximum is either at a location in the observation plane on the model or at a certain position in wave-number space. The associated cross correlation matrix is subtracted from the matrix $\boldsymbol{R}$ and added to either $\boldsymbol{R_1}$ or $\boldsymbol{R_2}$, depending on whether the maximum was in the source map or in the map in wave-number space. The whole cycle is repeated until the absolute maximum is below a certain threshold. In a last step the remaining matrix $\boldsymbol{R}$ is added to the accumulated matrix $\boldsymbol{R_1}$. Thus, the sum of the final matrices $\boldsymbol{R_1}$ and $\boldsymbol{R_2}$ corresponds to the initial cross spectral matrix. To calculate an improved source map, the matrix $\boldsymbol{R_1}$ is taken instead of the initial cross spectral matrix $\boldsymbol{R}$.

FIG 4 shows an example of measurements in a closed test section. The source map on the left shows a result calculated using the standard delay-and-sum beamforming including DR. In this case the angle of attack of the model is $\alpha = 7°$ and the flow velocity

u_{oo} = 30 m/s. The frequency of the source map is f = 2900 Hz (narrow band). x and y are local coordinates in the observation plane, which corresponds to the main plane of the wing and is rotated with the model. The local coordinate system is also rotated, so that the model appears upside down and the main flow direction points from left to right.

The strongest intensity in the source maps is found downstream of the wing. Some sources at the slat of the wing are visible, but they are much weaker than the sources at the right border of the maps directly downstream of the trailing edge. It appears unrealistic that real sources are present in this area. Thus, the high intensity downstream of the wing is more likely an artefact rather than it is caused by real sources in the observation plane.

The improved source map with the BiClean algorithm is shown on the right side in FIG 4. Now, the sources at the slat are dominating the whole map. The strong sources downstream of the wing have disappeared. These result shows that the proposed iterative method is able to reduce these artefacts or remove them almost completely.

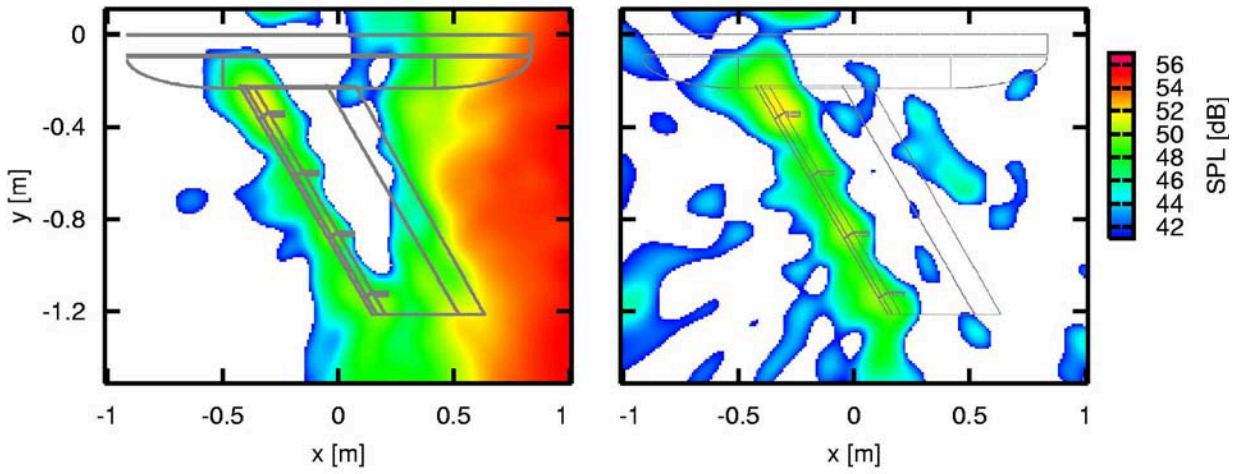

FIG 4. Source map at narrow band frequency f = 2900 Hz. The measurements were performed in a closed test section of the Technical University of Berlin with a swept constant chord half-model. Flow velocity is u_{oo} = 30 m/s and angle of attack α = 7°. Left: source maps are calculates by using the standard DSB, right: BiClean algorithm is applied to the cross correlation matrix before using the standard DSB.

3.3. Deconvolution

The array result and especially the resolution of the microphone array depends on the point spread function (or array pattern) of the microphone array (see section 2.3). The array output is contaminated with the sidelobes and the finite width of the mainlobe makes it sometimes difficult to interpret the array result. The ideal answer of the microphone array to a point source located at the position $\vec{y}_o$ would be the delta function $\delta(\vec{y}-\vec{y}_o)$. In that case, the beamforming output would reproduce the true source strength distribution $q(\vec{y})$. The fact that the point spread function in the case of a finite pressure sensitive area is not a delta function creates the need for deconvolution algorithms.

The idea of the deconvolution algorithms is to remove the side lobes and resolution effects from the beamforming result by inverse methods. In the acoustic-array community the introduction of the DAMAS (Deconvolution Approach for the Mapping of Acoustic Sources) algorithm by Brooks and Humphreys [8] drew the attention back to deconvolution as a possibility to increase the resolution of acoustic arrays and to get rid of disturbing side-lobe effects. In many fields of imaging, like for example optical and radio astronomy or optical microscopy, deconvolution methods are widely used to increase the spatial resolution. For that purpose a variety of algorithms has been developed in the past. These are classical approaches like the CLEAN algorithm introduced by Högbom [9]. Dougherty and Stoker [10] first applied the CLEAN algorithm in acoustic array measurements. The original DAMAS algorithm was simplified in the following DAMAS2 and DAMAS3 algorithms introduced by Dougherty [11]. A faster solution of the original DAMAS algorithm can be found in [12] and recently Sijtsma introduced an improved CLEAN algorithm which avoids the calculation of an artificial array pattern [14].

The mathematical formulation of these algorithms is very complex and will not be given here. In the following some results from [12] with synthetic signals and from [14] for measurement data will show the performance of two different deconvolution algorithms.

FIG 5 shows the synthetic source distribution $q(\vec{y})$ which has been used for the deconvolution analysis. The yellow lines consist of 160 grid points. In each of these points a source with unit strength is placed. The result calculated with a standard DSB is shown in FIG 6 on the left. The positions of the microphones for this simulation are the same as in FIG 1. The observation plane is parallel to the array plane and the distance between the microphones and the plane of the simulated sources in FIG 6 is 1 m. Such a value is typical for the experiments which are performed with the DLR in-flow array. The signal frequency is f = 3 kHz.

The wedge structure is clearly visible in the source map but the small square structure is heavily blurred. The ratio between the peak signal and the background noise is about 10 to 15 dB.

In the next step the deconvolution algorithm (embedded DAMAS2 proposed in [12]) is applied to this test case. The source distributions reconstructed by this algorithm are shown in FIG 6 on the right. It can be seen that the reconstructed distribution improves significantly for this advanced deconvolution algorithm. Even the background noise in the outer regions is reduced. The square structure is almost completely recovered. The background values inside the square are lowered by more than 20 dB and the square is clearly recognizable.

In the following recent results from Sijtsma [14] show that the deconvolution algorithms can also be used to improve results from wind tunnel measurements. FIG 7 shows results of Airbus A340 array measurements (1:10.6 scale model) in the 8 x 6 m^2 closed test section of DNW-LLF. These tests were carried out within the EU-project AWIATOR. Measurements were done with a wall-mounted array of 128 microphones, underneath the starboard wing.

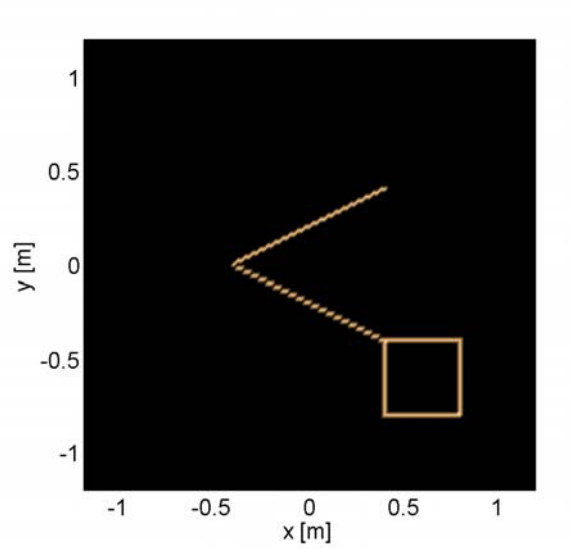

FIG 5. Pre-given synthetic source distribution. The yellow lines consist of 160 grid points. In each of these points a source with unit strength is placed.

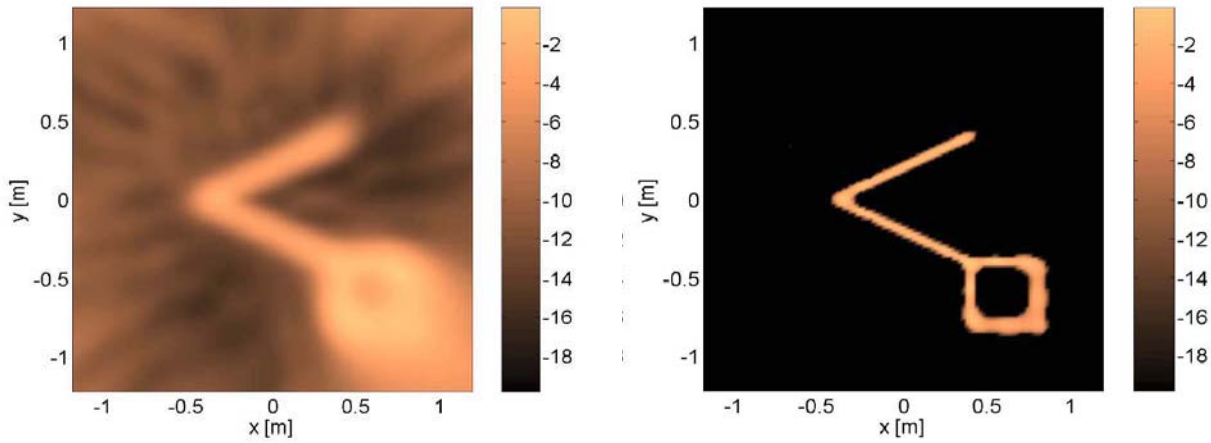

FIG 6. Results calculated using the pre-given source distribution in FIG 5. Left: Calculation using the standard DSB. Right: embedded DAMAS2 algorithms from [12]. The microphone arrangement is in both cases the same as in FIG 1.

For a typical configuration at 60 m/s wind speed, source plots obtained with the standard delay-and-sum beamformer (with diagonal removal) are shown in FIG 7. For comparison FIG 8 shows the result with the CLEAN-SC deconvolution algorithm proposed in [14]. In both cases the 3rd octave bands with the centre frequencies f_m = 6.3 kHz, f_m = 8 kHz and f_m = 10 kHz are shown. At these frequencies a significant improvement in spatial resolution is observed. At the leading edge, regularly spaced sources can be observed, which coincide with the slat tracks. Another advantage of the proposed deconvolution algorithm is that the side lobes of the array pattern are removed from the source maps. Therefore the absolute values calculated on the basis of these source maps are more reliable.

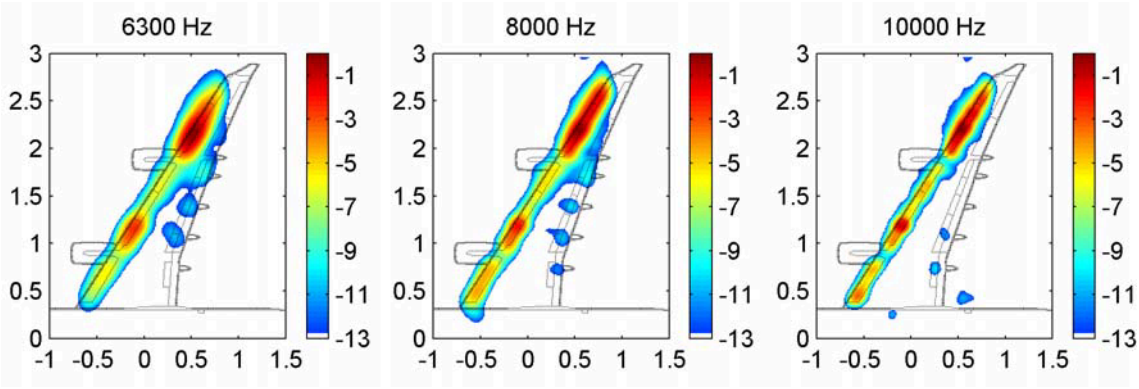

FIG 7. Source maps of a A340 scale model at 60 m/s wind speed. The maps were calculates using a standard DSB with diagonal removal. Depicted are the 3rd octave bands with the centre frequency fm = 6.3 kHz, fm = 8 kHz and fm = 10 kHz.

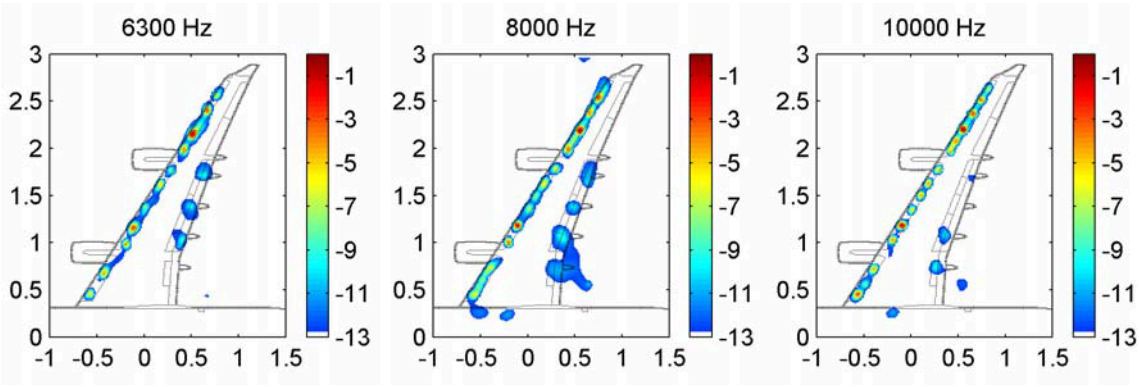

FIG 8. Source maps of a A340 scale model at 60 m/s wind speed. The maps were calculated using the CLEAN-SC deconvolution algorithm. Depicted are the 3rd octave bands with the centre frequency fm = 6.3 kHz, fm = 8 kHz and fm = 10 kHz..

4. PRACTICAL APPLICATION OF MICORPHONE ARRAY MEASUREMENTS

In this section some practical aspects for microphone array measurements in the closed test section are summarized. In section 4.1 two examples of typical measurement setups are shown. In the following section 4.2 the basic requirements of the data acquisition are given. The software to control the measurement and the data analysis is illustrated in section 4.3.

4.1. Measurement setup

A typical microphone-array measurement setup in the low speed facility of DNW (DNW-LST) is shown in FIG 9. It is a closed circuit type atmospheric wind tunnel with a contraction ratio of 9 and a maximum velocity of 80 m/s. The dimensions of the test section are: width 3.0 m and height 2.25 m. The NLR/DNW microphone array is mounted to the side wall of the test section so that the sound waves radiated from the pressure side of the model can be recorded by the microphones. The 96 array microphones were mounted flush in the red support plate, within a surface of 57 cm × 44 cm. The array output was calculated between 4 and 55 kHz.

FIG 10 shows the noise source distributions as determined for the landing configurations at flow velocity u_{oo} = 75 m/s and frequency f_m = 20 kHz. Compared are the configurations with and without a fence device to reduce the flap side-edge noise. The (local) noise source distribution is given in terms of the sound power levels, expressed in decibels re 1 pW. FIG 10 clearly illustrates that the flap side-edge noise is reduced by approx. 6 dB in this 3rd octave band by this noise reduction device. This example shows that the microphone array is a very powerful tool in wind tunnel measurements to develop and improve noise reduction strategies.

FIG 11 illustrates the setup of a microphone-array measurement in an industrial wind tunnel. The picture shows the closed test section of the low speed facility of AIRBUS Bremen (BLSWT). The DLR microphone array is mounted to the side wall of the test section. The distance between array and model is approx. 0.9 m and the dimensions of the microphone array are: length 1.7 m and height 1.3 m. The thickness of the array

casing is 25 mm. 144 microphones are integrated into the array casing. The arrangement of the microphones is shown in FIG 1. The microphones are recessed to reduce the pressure fluctuations of the turbulent boundary layer which develops over the microphone array.

FIG 9. Typical microphone-array measurement setup in the low speed facility of DNW (DNW-LST). The DNW microphone array is mounted to the side wall of the test section.

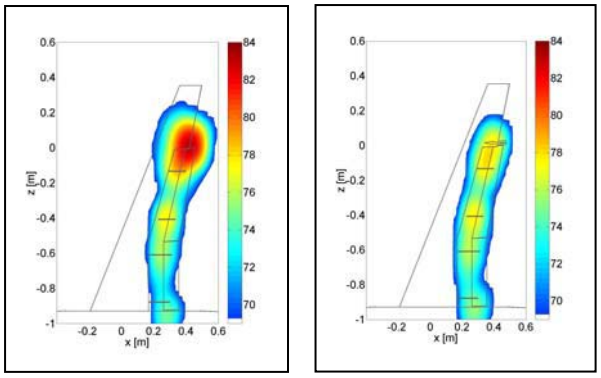

FIG 10 Result from microphone array measurements shown in FIG 9. Compared are flap side-edge measurements without (left) and with (right) side edge fence.

FIG 11. Microphone-array measurements in the closed test section of the low speed facility of AIRBUS Bremen (BLSWT). The DLR microphone array is mounted to the side wall of the test section.

This setup will be used for the array measurements within the EWA benchmark-test described in the introduction.

4.2. Data acquisition system

The wind tunnel models used for aero acoustic testing are usually scaled down. Therefore very high frequencies have to be sampled by the data acquisition system. The NLR/DNW- and the DLR-acquisition system allow a sampling frequency up to 250 kHz per channel which results in a frequency bandwidth of 100 kHz. Each channel of the data acquisition system is equipped with three different programmable signal amplifiers. The overall gain can be adjusted between 0.5 and 500000. An automatic auto-range feature can select the optimum gain individually for each channel.

FIG 12. DLR data acquisition system. The picture shows three units which comprise 144 channels.

FIG 12 shows three acquisition units from the DLR data acquisition system. Each data acquisition unit can capture up to 48 channels and store the captured data on a local hard disk. Combining all data acquisition units from DNW, NLR and DLR measurements with up to 624 channels are possible.

The acquisition time of this system is only limited by the capacity of the storage medium in each unit. This allows the recording of long measurement sequences and therefore a large number of averages in the array analysis. Because of this averaging process, the pressure fluctuations, caused by the unsteady flow in the turbulent boundary layer, are effectively suppressed.

4.3. Control of measurement and analysis

The data acquisition system is controlled via a TCP/IP network connection. Therefore, the measurement can be triggered from a remote master PC. In industrial

applications it is often required that a large number of data points are recorded and the exact moment of each measurement depends on the aerodynamic configuration in the test section. Furthermore, the respective parameters for each measurement like flow velocity, angle of attack and temperature have to be stored together with the measured data. Therefore, it is very useful to establish a connection between the data acquisition and the wind-tunnel control-system. This has been done both by DLR and by DNW/NLR.

As an example FIG 13 shows the structure of the DLR data-acquisition and analysis control-system. If the control system is set to *measurement* the data acquisition control system is waiting for a certain file which has to be generated by the wind tunnel control system and written to a defined directory. The generation of this file is the trigger for the acquisition system to start the measurement. Moreover, this trigger file contains the parameters of the measurement (flow velocity, temperature etc.). The data acquisition control system sends the start flag to the data acquisition units that record the microphone signals for a defined period of time. When the measurement is finished the DAs send a ready signal to the DA control which in turn deletes the trigger file, thus passing the ready information to the WT control system. The DA system is now ready for the next data point.

The second part in the network is the array manager (AM) that controls the array analysis and data backup. The data of the DAs is stored after each measurement on a RAID system and in parallel on the processing PC that performs the array analysis. These procedures are controlled by the AM. For this purpose the AM also gets the wind tunnel parameters after each measurement from the DA control. The important point is that the two control systems work independently from each other so that an efficient measurement procedure is guaranteed. The array processing is done in parallel to the measurements, and array results are typically available within 10 minutes after the measurement (conventional beamforming and power integration).

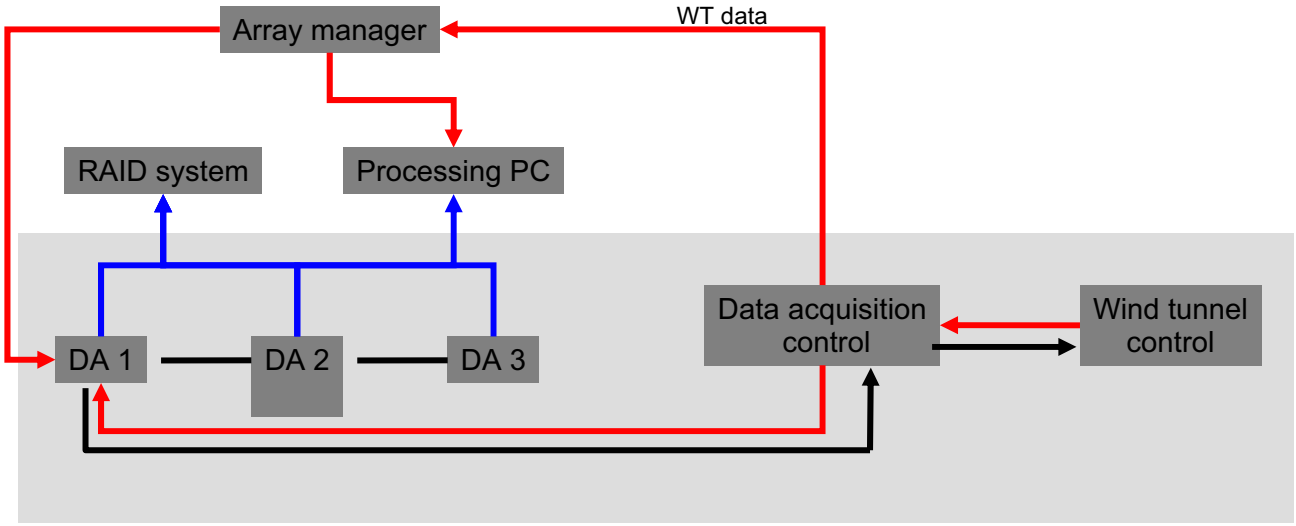

FIG 13. Structure of the DLR data-acquisition and processing system.

5. CONCLUSIONS AND FUTURE DEVELOPMENTS

This paper shows that the microphone array measurement technique has been developed as a technically mature approach to measure sound radiated from aircraft models in closed test sections. The basic problems like disturbing boundary layer and background noise and limited spatial resolution have been solved by the European research institutes. Others like measurement of moving sources [21] and sound wave reflections ([3], [6]) have not been mentioned here for lack of space. In addition, some practical aspects for microphone array measurements in the closed test section have been illustrated. A high standard in data acquisition and hardware setup has been established by European research institutes.

As stated in the introduction the major objective is to extract far-field data from microphone array measurements in the closed test section. The present costs for aero acoustic tests could be reduced considerably by this approach due to the fact that the number of fly-over tests with real aircrafts can be reduced and the development of noise reduction design concepts can be integrated in the aerodynamic design process. The future activities and developments which are required for this objective are:

- Development of an in-site calibration procedure to calibrate microphone arrays in the closed test section. The requirements for the calibration source are: omni-directional or at least known directivity and sufficient amplitude in a large frequency range.
- The directivity of the measured sound sources on

the model has to be considered in the measurement setup. Either the position of the array in the test section has to be adjusted to the given angle of attack of the model or the size of the array has to be increased. In the latter case the pressure sensitive area of the microphone array has to be adjusted to the given configuration electronically by bank switching.

- The directivity (amplitude and phase) of the microphones has to be incorporated into the analysis process.
- Furthermore to determine the absolute far-field sound pressure level from wind tunnel measurements model effects have to be considered in the future. For design-engineering reasons the dimensions of aircraft models are not exactly the scaled versions of the real aircraft. The design of the slat or the flap tracks of aircraft models for example is usually much simpler than the ones on the real aircraft. This might lead to a different sound pressure level in microphone array measurements compared to fly-over measurements. The same is true for Re-number effects. Some aero acoustic sound sources are for example caused by a laminar separation. In this case the source is not measured accurately if the model Re-number does not correspond to the Re-number of the real aircraft.
- In industrial applications of the array technique the data-processing time is a critical parameter. Especially if advanced algorithms like the BiClean or the Deconvolution algorithms are used as a standard procedure the software codes have to be parallelized in the near future.

6. OUTLOOK

In order to find solutions to the problems mentioned above partners of the EWA consortium such as NLR, DNW, ONERA and DLR have chosen a two step approach. First a measurement of the noise generated by a model in high-lift configuration such as depicted in FIG 11 will be performed with a single microphone-array. In the second step all partners will perform the analysis of this dataset using their in-house software. By comparing and evaluating the results as obtained with the different software implementations considerable new insights into accuracy and repeatability are to be expected. Joint efforts by all EWA partners developing the phased-array technique will lead to a much faster progress than achievable by a single partner alone.

7. REFERENCES

[1] L. Koop, K. Ehrenfried, A. Dillmann and U. Michel, Reduction of flap side edge noiseby active flow control, AIAA paper 20022469,2002.
[2] P. Sijtsma and H. Holthusen, Source location by phased measurements in closed wind tunnel test sections, AIAA Paper 99-1814, 1999.
[3] S. Guidati, C. Brauer and S. Wagner, The Reflection Canceller – Phased array measurements in a reverberating environment, AIAA Paper 2002-2462, 2002.
[4] H. van der Wal and P. Sijtsma, Flap noise measurements in a closed wind tunnel with a phased array, AIAA paper 2001-2170, 2001.
[5] K. Ehrenfried, L. Koop, A. Henning and K. Kaepernick, Effects of Wind-Tunnel Noise on Array Measurements in Closed Test Sections. First Berlin Beamforming Conference 2006, Berlin, 2006.
[6] P. Sijtsma. Corrections for Mirror Sources in Phased Array Processing Techniques, AIAA paper 2003-3196, 2004
[7] D. Blacodon and G. Elias, Level Estimation of Extended Acoustic Sources using a Parametric Method, Journal of Aircraft, Vol. 41, No. 6, November–December 2004.
[8] T. F. Brooks and Humphreys, W.M., A Deconvolution Approach for the Mapping of Acoustic Sources (DAMAS) Determined from Phased Microphone Arrays, Journal of Sound and Vibration, Vol. 294, March 2006, pp. 856-879, also AIAA Paper 2004-2954, May 2004.
[9] J. Högbom, Aperture syntheses with a non-regular distribution of interferometer baselines, Astron. Astrophys. Suppl., Vol. 15, 1974, pp. 417–426.
[10] R. P. Dougherty and R. W. Stoker, Sidelobe Suppression for Phased Array Aeroacoustic Measurements, AIAA Paper 98-2242, June 1998.
[11] R. P. Dougherty, Extensions of DAMAS and Benefits and Limitations of Deconvolution in Beamforming, AIAA Paper 2005-2961, May 2005.
[12] K. Ehrenfried and L. Koop, A Comparison of Iterative Deconvolution Algorithms for the Mapping of Acoustic Sources, AIAA Paper 2006-2711, 2006.
[13] S. Oerlemans, L. Broersma and P. Sijtsma, Quantification of airframe noise using microphone arrays in open and closed wind tunnels, submitted to International Journal of Aeroacoustics, Nov. 2006.
[14] P. Sijtsma, CLEAN Based on Spatial Source Coherence, AIAA paper 2007-3436, 2007.
[15] F. F. Piet and G. Elias, Airframe noise source localization using a microphone array, AIAA Paper 97-1643, 1997.
[16] P. Sijtsma and H. Holthusen, Source location by phased measurements in closed wind tunnel test sections, AIAA Paper 99-1814, 1999
[17] U. Michel, B. Barsikow, J. Helbig, M. Hellmig and M. Schüttpelz, Flyover Noise Measurements on a Landing Aircraft with a Microphone Array, 4th AIAA/CEAS Aeroacoustics Conference, No. AIAA-Paper 98-2224, Toulouse, France, 1998.
[18] S. Oerlemans and P. Sijtsma, Determination of Absolute Levels from Phased Array Measurements using Spatial Coherence, AIAA Paper 2002-2464, June 2002.
[19] T. F. Brooks and W. M. Humphreys, Effect of Directional Array Size on the Measurement of Airframe Noise Components, AIAA Paper 99-1958, May 1999.
[20] R. P. Dougherty, Source Location with Sparse Acoustic Arrays; Interference Cancellation, Presented at the First CEAS-ASC Workshop: Wind Tunnel Testing in Aeroacoustics, DNW, 5-6 November 1997.
[21] P. Sijtsma, S. Oerlemans and H. Holthusen, Location of rotating sources by phased array measurements, AIAA Paper 2001-2167, NLR-TP-2001-135, May 2001.